Available online at www.sciencedirect.com
SCIENCE DIRECT
Journal of Sound and Vibration 297 (2006) 37–54
JOURNAL OF SOUND AND VIBRATION
www.elsevier.com/locate/jsvi

Modelling of floating-slab tracks with continuous slabs under oscillating moving loads

M.F.M. Hussein*, H.E.M. Hunt

Engineering Department, Cambridge University, Trumpington Street, Cambridge CB2 1PZ, UK

Received 7 October 2005; received in revised form 7 February 2006; accepted 13 March 2006
Available online 30 May 2006

Abstract

This paper discusses modelling of floating-slab tracks on rigid foundations. The model consists of an upper Euler–Bernoulli beam to account for both the rails and a lower Euler–Bernoulli beam to account for the slab. There are two continuous resilient layers in the model: one to account for railpads between the rails and the slab and one to account for slab-bearings underneath the slab. The Fourier transformation method is used to calculate displacements of such a track under an oscillating moving load. These results are used to calculate the cut-on frequencies and critical velocity of the track. The work in this paper also demonstrates some basic concepts in the context of vibration of infinite systems including dispersion curves, critical velocities, load-velocity lines and coupling of systems in the wavenumber-frequency domain. The paper offers a complete treatment of the issues important to the analysis of a double-beam system not elsewhere available in the published literature.

1. Introduction

Floating-slab tracks are widely used to control vibration from underground trains [1–4]. The track is mounted on a concrete slab that rests on rubber bearings, glass fibre, or steel springs. The slab may be cast in situ, resulting in a continuous length of concrete, or may be constructed in discrete pre-cast sections laid end to end. Examples of floating-slab tracks are, among others, the 1.5 m slab in Toronto, the 3.4 m Eisenmann track in Munich and Frankfurt, the 7 m slab in New York subway and the WMATA continuous slab system in Washington DC.

This paper addresses modelling of floating-slab tracks with continuous slabs. The principal components relevant to vibration modelling are the rails, the railpads, the floating slab and the slab bearings. The track-bed is modelled as a rigid foundation, as the stiffness of slab bearings is normally much smaller than the stiffness of the track-bed. For a soft track-bed, however, the stiffness of the ground can be incorporated in the model by considering the total stiffness resulting from the stiffness of slab bearings in series with the stiffness of the track-bed. The rigid-bed models are useful as quick tools to investigate the wheel–track interaction and can be

*Corresponding author. Tel.: +44 1223 765925; fax: +44 1223 332662.
E-mail addresses: mfmh2@cam.ac.uk (M.F.M. Hussein), hemh1@cam.ac.uk (H.E.M. Hunt).

0022-460X/$ - see front matter © 2006 Elsevier Ltd. All rights reserved.
doi:10.1016/j.jsv.2006.03.026

used in sub-modelling, i.e. to calculate the ground-borne vibration by using the calculated forces at the track-bed as an input to a different model which accounts for the tunnel and the ground.

There are many models presented in the literature for railway tracks on rigid foundation. One of the oldest and most widely accepted models, sometimes known as a beam on elastic foundation, was first presented by Winkler in 1867. The model consists of a single infinite beam supported on a foundation with constant stiffness [5]. There are two formulations used to account for the beam's behaviour: Euler–Bernoulli and Timoshenko. The former accounts only for bending while the latter accounts also for shear deformations and rotary inertia [6]. For a low frequency of excitation, where the propagating wave has a wavelength much greater than the beam-cross-sectional dimensions, both formulations converge to the same solution. For a high frequency of excitation, Timoshenko formulation is necessary for an accurate solution.

The steady-state vibration of an undamped beam on elastic foundation due to a non-oscillating moving load is investigated by many authors [7–10]. The solution for the damped case is presented by Kenny [11] to account for velocities above the critical velocity of the beam.

The work of Mathews [12,13] calculates the steady-state response of an Euler–Bernoulli beam on an elastic foundation under an oscillating moving load. The Fourier transformation is used to calculate a closed form solution for the response using contour integrals and the residue theorem. Analysis of the same problem but using Timoshenko formulation can be found in Chonan [14]. Bogacz et al. [15] present a generalization of the problem comparing results of the beam response calculated by the two formulations.

In the previous models, viscous damping is used whenever damping is introduced to the foundation. However, structural damping may also be used [16] to account for energy losses. A detailed study of modelling of infinite beams, and finite beams, under oscillating moving loads can be found in Ref. [17].

A more complicated problem in which the complete solution (transient and steady state) of a beam on elastic foundation under an oscillating moving mass, is calculated by Duffy [18]. Fourier transformation is used to transform the differential equation with respect to space, while Laplace transformation is used with respect to time.

There are other less popular types of foundations used in the literature. Example is Pasternak foundation which is a Winkler foundation with a shear layer coupled from the top [19]. A recent study by Mallik et al. [20] shows that there are insignificant differences between the results of Winkler and Pasternak foundations for a beam subjected to a static moving load.

The literature on modelling of double beams is extensive on finite lengths with only one layer of resilient between the two beams. For example, Kessel [21] studies the eigenfrequencies of a simply supported double-beam system under an oscillating moving load. The complete solution of a finite double beam is calculated by Vu et al. [22]. Different formulations of a beam, such as Euler–Bernoulli and Timoshenko, are used by Han et al. [23] to calculate the dynamics of a vibrating double beam with different set of boundary conditions.

Chen and Shiu [24] used a method based on the dynamic stiffness matrices to account for an elevated railway subjected to harmonic moving loads. Three different models are presented, two of them are relevant to the literature presented here. One model is a double-beam system that is simply supported. Another is a double-beam system connected from its sides by two semi-infinite beams on elastic foundations.

Cui and Chew [25] use the Laplace transformation method to model two different tracks in the Singapore mass rapid transit (SMRT) system. Both tracks are analysed using infinitely long two-dimensional (2D) models on rigid foundations. The first is a fixed track slab, modelled as a beam on elastic foundation. The second is a floating-slab track with discontinuous slab modelled as a beam supported elastically on continuous masses on elastic foundation.

Modelling of floating-slab tracks on rigid foundation under oscillating loads is presented by Forrest [4]. His work considers only oscillating loads that are fixed in position with no attempt to account for moving loads. A direct solution, presented in the appendix of this paper, based on separable functions in time and space is followed to solve the differential equation for a track with a continuous slab. For a track with discontinuous slabs, the repeating unit method is used which incorporates Floquet's theorem to account for periodicity of the track. One of the findings of the work [4,26] is that the ratio between the total transmitted force to the ground and the input force is equal to the transmissibility calculated from a two-degree-of-freedom (2dof) system. This finding holds for tracks with continuous and discontinuous slabs.

In this paper, the work of Forrest on modelling of tracks with continuous slabs is extended to account for moving loads. The analytical background is presented in Section 2 while the results and discussion are given in Section 3. It may be useful for readers to go first through the appendix as it presents a complete demonstration of some of the basic concepts that simplify understanding the contents of Sections 2 and 3.

2. Modelling of tracks with continuous slabs

In this section, analysis is carried out for a floating-slab track with continuous slab subjected to an oscillating moving load with angular frequency ϖ and velocity v. The model is shown in Fig. 1. It consists of an upper Euler–Bernoulli beam to account for both of the rails (with mass m_1 per unit length and bending stiffness EI_1) and a lower Euler–Bernoulli beam to account for the floating slab (with mass m_2 per unit length and bending stiffness EI_2). The model accounts for identical inputs on the two rails and hence a single beam is used to model both of the rails. Railpads are represented by a continuous layer of springs with stiffness k_1 per unit length and a viscous damping factor c_1 per unit length. Slab bearings are represented by a continuous layer of springs with stiffness k_2 per unit length and a viscous damping factor c_2 per unit length. The space–time coordinates are defined in a way that the load passes by $x = 0$ at time $t = 0$. The solution methodology depends on transforming the differential equations of the track to the wavenumber-frequency domain, where they are simplified and transformed back to the space–time domain. The reader is referred to the appendix for a detailed description of the method.

The load on the upper beam in Fig. 1 can be written in the space–time domain as follows

$$F(x,t) = \mathrm{e}^{\mathrm{i}\varpi t}\delta(x - vt), \tag{1}$$

where δ is the *Dirac delta* function, see Ref. [27] for example. The generalised differential equations of the upper and the lower beams can be written as

$$EI_1\frac{\partial^4 y_1}{\partial x^4} + m_1\frac{\partial^2 y_1}{\partial t^2} + k_1(y_1 - y_2) + c_1\left(\frac{\partial y_1}{\partial t} - \frac{\partial y_2}{\partial t}\right) = \mathrm{e}^{\mathrm{i}\varpi t}\delta(x - vt) \tag{2}$$

and

$$EI_2\frac{\partial^4 y_2}{\partial x^4} + m_2\frac{\partial^2 y_2}{\partial t^2} + k_2 y_2 - k_1(y_1 - y_2) + c_2\frac{\partial y_2}{\partial t} - c_1\left(\frac{\partial y_1}{\partial t} - \frac{\partial y_2}{\partial t}\right) = 0. \tag{3}$$

When solving problems of moving loads, some authors prefer at this stage to replace the fixed frame of axis, i.e. (x, t), by the moving frame of axis, i.e. $(z = x - vt, t)$, see [17] for example. However, the derivation without following this approach leads to the same results at the end and has the advantage of giving more insight into defining the *critical velocity* which is discussed in Section 3. Eqs. (2) and (3) are transformed from the space–time domain (x,t) to the wavenumber-frequency domain (ξ,ω) using double Fourier transform, see Ref. [28] for example. The transformed equations read

$$EI_1\xi^4\tilde{y}_1 - m_1\omega^2\tilde{y}_1 + k_1(\tilde{y}_1 - \tilde{y}_2) + c_1 i\omega(\tilde{y}_1 - \tilde{y}_2) = 2\pi\delta(\omega + \xi v - \varpi), \tag{4}$$

and

$$EI_2\xi^4\tilde{y}_2 - m_2\omega^2\tilde{y}_2 + k_2\tilde{y}_2 - k_1(\tilde{y}_1 - \tilde{y}_2) + c_2 i\omega\tilde{y}_2 - c_1 i\omega(\tilde{y}_1 - \tilde{y}_2) = 0, \tag{5}$$

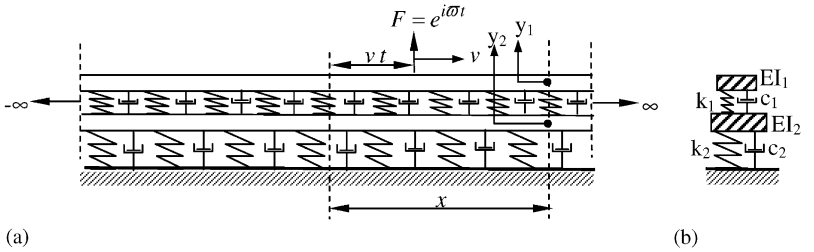

Fig. 1. (a) Floating-slab track on a rigid foundation, subjected to a unit moving oscillating load and (b) side view.

where $\tilde{y}_1$ and $\tilde{y}_2$ are the transformation of y_1 and y_2 in the wavenumber-frequency domain. Eqs. (4) and (5) can be written in matrix form as

$$\mathbf{A}\begin{bmatrix}\tilde{y}_1\\ \tilde{y}_2\end{bmatrix}=\begin{bmatrix}2\pi\delta(\omega+\xi v-\varpi)\\ 0\end{bmatrix}, \tag{6}$$

where

$$\mathbf{A}=\begin{bmatrix}EI_1\xi^4-m_1\omega^2+k_1+c_1i\omega & -k_1-c_1i\omega\\ -k_1-c_1i\omega & EI_2\xi^4-m_2\omega^2+k_1+k_2+i\omega(c_1+c_2)\end{bmatrix}.$$

Solving for $\tilde{y}_1, \tilde{y}_2$ from Eq. (6)

$$\tilde{y}_1(\xi,\omega)=\frac{2\pi\delta(\omega+\xi v-\varpi)f_2(\xi,\omega)}{f_1(\xi,\omega)} \tag{7}$$

and

$$\tilde{y}_2(\xi,\omega)=\frac{2\pi\delta(\omega+\xi v-\varpi)f_3(\xi,\omega)}{f_1(\xi,\omega)}, \tag{8}$$

where $f_1(\xi,\omega)=|\mathbf{A}|$, $f_2(\xi,\omega)=EI_2\xi^4-m_2\omega^2+k_1+k_2+i\omega(c_1+c_2)$, $f_3(\xi,\omega)=k_1+c_1i\omega$ and $|\mathbf{A}|$ is the determinant of matrix $\mathbf{A}$. Eqs. (7) and (8) are transformed to the wavenumber-time domain firstly, resulting in

$$\bar{y}_1(\xi,t)=\frac{f_2(\xi,\omega=\varpi-\xi v)}{f_1(\xi,\omega=\varpi-\xi v)}e^{i(\varpi-\xi v)t} \tag{9}$$

and

$$\bar{y}_2(\xi,t)=\frac{f_3(\xi,\omega=\varpi-\xi v)}{f_1(\xi,\omega=\varpi-\xi v)}e^{i(\varpi-\xi v)t}. \tag{10}$$

Transforming Eqs. (9) and (10) from the wavenumber-time domain to the space–time domain results in

$$y_1(x,t)=\frac{e^{i\varpi t}}{2\pi}\int_{-\infty}^{\infty}\frac{f_2(\xi,\omega=\varpi-\xi v)}{f_1(\xi,\omega=\varpi-\xi v)}e^{i\xi(x-vt)}\,d\xi \tag{11}$$

and

$$y_2(x,t)=\frac{e^{i\varpi t}}{2\pi}\int_{-\infty}^{\infty}\frac{f_3(\xi,\omega=\varpi-\xi v)}{f_1(\xi,\omega=\varpi-\xi v)}e^{i\xi(x-vt)}\,d\xi. \tag{12}$$

The previous integrations can be performed numerically along the real ξ-axis. Otherwise, this integration is carried out analytically using the contour integrals, see the appendix for more details. $f_1(\xi,\omega)$ is a polynomial of the eighth order and hence the integrated functions in Eqs. (11) and (12) have eight poles. All these poles are complex values if any of c_1 or c_2 is not equal zero. The integrations in Eqs. (11) and (12) can be written as

$$y_1(x,t)=\frac{ie^{i\varpi t}}{EI_1EI_2}\sum_{n=1}^{4}\frac{e^{i\xi_n(x-vt)}f_2(\xi_n,\omega=\varpi-\xi_n v)}{\prod_n}\quad\text{for } x-vt>0, \tag{13}$$

$$y_2(x,t)=\frac{ie^{i\varpi t}}{EI_1EI_2}\sum_{n=1}^{4}\frac{e^{i\xi_n(x-vt)}f_3(\xi_n,\omega=\varpi-\xi_n v)}{\prod_n}\quad\text{for } x-vt>0, \tag{14}$$

$$y_1(x,t)=\frac{-ie^{i\varpi t}}{EI_1EI_2}\sum_{n=5}^{8}\frac{e^{i\xi_n(x-vt)}f_2(\xi_n,\omega=\varpi-\xi_n v)}{\prod_n}\quad\text{for } x-vt<0, \tag{15}$$

and

$$y_2(x,t) = \frac{-i\mathrm{e}^{\mathrm{i}\varpi t}}{EI_1EI_2}\sum_{n=5}^{8}\frac{\mathrm{e}^{\mathrm{i}\xi_n(x-vt)}f_3(\xi_n,\omega=\varpi-\xi_n v)}{\prod_n} \quad \text{for } x-vt<0, \tag{16}$$

where

$$\prod_n = (\xi_n-\xi_1)(\xi_n-\xi_2)\ldots(\xi_n-\xi_{n-1})(\xi_n-\xi_{n+1})\ldots(\xi_n-\xi_8),$$

$\xi_1, \xi_2, \ldots, \xi_8$ are the roots of the equation $f_1(\xi,\omega=\varpi-\xi v)=0$, ξ_1, ξ_2, ξ_3, ξ_4 are the roots in the first and the second quadrants, and ξ_5, ξ_6, ξ_7, ξ_8 are the roots in the third and the fourth quadrants.

3. Results and discussions

The parameters used to analyse floating-slab tracks are given in Table 1. These parameters are identical to the ones used by Forrest [4] except for the dampers. Smaller damping factors are used with damping ratios ζ of 5% which is a typical value for an isolation pad. The damping factors can be calculated from the damping ratios from the following relationships:

$$c_1 = 2\zeta_1\sqrt{k_1m_1} \quad \text{and} \quad c_2 = 2\zeta_2\sqrt{k_2m_2}. \tag{17}$$

The free-vibration equations of a floating-slab track are calculated from Eq. (6) by setting the force to zero, i.e.

$$\mathbf{A}\tilde{\mathbf{y}} = \mathbf{A}\begin{bmatrix}\tilde{y}_1\\ \tilde{y}_2\end{bmatrix} = \begin{bmatrix}0\\0\end{bmatrix}. \tag{18}$$

The dispersion equation is calculated by the non-trivial solution of this equation, i.e. $|\mathbf{A}|=0$ or $f_1(\xi,\omega)=0$ as in Eq. (7) and (8) with $c_1=0$ and $c_2=0$ (compare with Eq. (A.21)). The vector $\tilde{\mathbf{y}}$ is the eigenvector describing the mode shape and can be calculated as explained in the appendix. The dispersion curves are the real solutions of the dispersion equation and usually plotted for only positive frequencies due to symmetry about zero frequency. However, negative frequencies are important for calculation of critical velocities, which will be discussed later in this section.

Fig. 2 shows the dispersion curves of the track. It has two positive cut-on frequencies. The first occurs at 18.75 Hz, where waves start to propagate away from the excitation point. Note that cut-on frequencies of the track are associated with zero wavenumbers, i.e. infinite wavelengths, and hence the track behaves as a 2D structure. As the slab is much heavier than the rails, the value of the first cut-on frequency can also be approximately calculated using the single-degree-of-freedom (1dof) system consisting of a mass equal to the slab's mass per unit length and a spring with stiffness equal to the slab-bearings' stiffness per unit length, i.e. $f=1/(2\pi)\sqrt{k_2/m_2}$, which results in a cut-on frequency of 19.02 Hz. By calculating $\tilde{\mathbf{y}}$ in Eq. (18) at the first cut-on frequency, the motion of the rails and the slab is observed to be in phase.

The second cut-on frequency occurs at 102.15 Hz. At this cut-on frequency, waves propagate in which only the rails vibrate, while the slab does not move. Again the value of the second cut-on frequency can be approximately calculated using the 1dof system consisting of a mass equal to the rails' mass per unit length and a spring with stiffness equal to the railpads' stiffness per unit length, i.e. $f=1/(2\pi)\sqrt{k_1/m_1}$, which results in a cut-on frequency of 100.66 Hz.

Table 1
Parameter values used for the floating-slab track

Rail	Slab
$EI_1 = 10\times10^6\,\mathrm{Pa\,m^4}$	$EI_2 = 1430\times10^6\,\mathrm{Pa\,m^4}$
$m_1 = 100\,\mathrm{kg\,m^{-1}}$	$m_2 = 3500\,\mathrm{kg\,m^{-1}}$
$k_1 = 40\times10^6\,\mathrm{N\,m^{-2}}$	$k_2 = 50\times10^6\,\mathrm{N\,m^{-2}}$
$c_1 = 6.3\times10^3\,\mathrm{N\,s\,m^{-2}}$	$c_2 = 41.8\times10^3\,\mathrm{N\,s\,m^{-2}}$

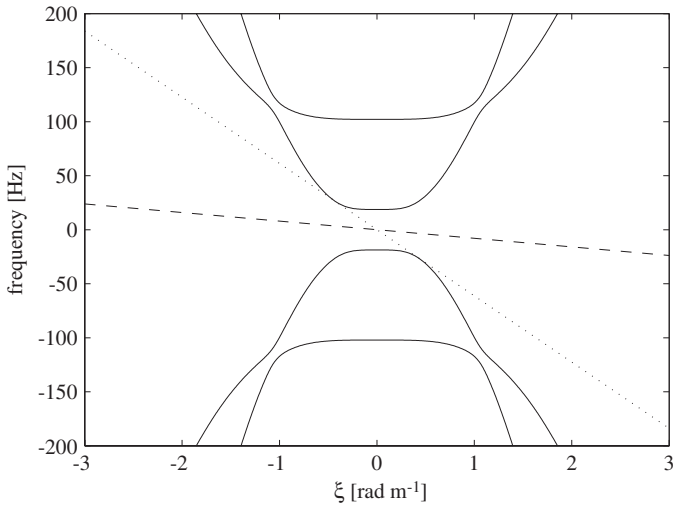

Fig. 2. Dispersion curves (——) of the floating-slab track calculated from the equation $f_1(\xi,\omega)=0$. The load velocity lines are also shown for two velocities $50\,\mathrm{m\,s^{-1}}$(- - - -) and $385\,\mathrm{m\,s^{-1}}$ ($\cdots$).

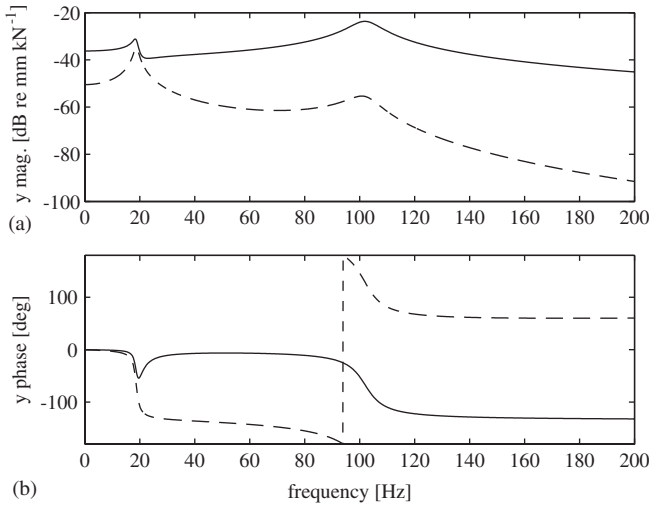

Fig. 3. Response of rails (——) and slab (- - - -) under a non-moving oscillating load: (a) displacement and (b) phase.

The track displacements under a static moving load, i.e. $\varpi=0$, can be evaluated by performing the integrations in Eqs. (11) and (12) numerically. Note that the integrated functions have infinite values at points where the denominator $f_1(\xi,\omega=-\xi v)=0$ is equal to zero. The dispersion curves in Fig. 2 give the solutions of the equation $f_1(\xi,\omega)=0$ in absence of damping. At the velocity when the line $\omega=-\xi v$ becomes tangential to the curve $f_1(\xi,\omega)=0$, the displacement becomes infinite and this velocity is called the critical velocity.

In the absence of damping, the displacement tends to infinity as the velocity approaches the critical velocity. If damping is included, the functions $f_2(\xi,\omega)/f_1(\xi,\omega)$ and $f_3(\xi,\omega)/f_1(\xi,\omega)$ will have peaks at the dispersion curves with higher values at lower angular frequencies ω. Hence, the track will have a finite peak at the critical velocity and smaller displacements at higher velocities. Fig. 2 shows the line $\omega=-\xi v$ which is called the *load-velocity line*, for two velocities; 50 and $385\,\mathrm{m\,s^{-1}}$. The latter is the track's critical load velocity.

Fig. 3(a and b) shows the track displacements and phases for a non-moving oscillating load. It can be seen that peaks occur at cut-on frequencies. This is because the load line $\omega=\varpi-\xi v$ (with $v=0$ in this case) becomes tangential to one of the dispersion curves of the track in Fig. 2 at cut-on frequencies. The importance

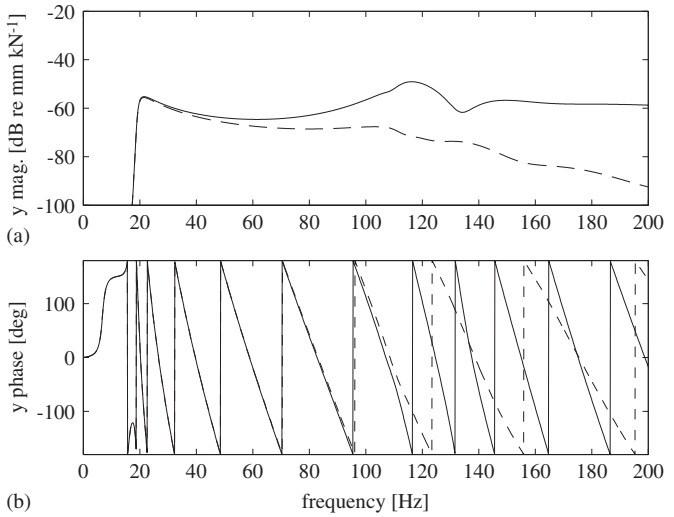

Fig. 4. Response of rails (——) and slab (- - - -) at 40 m away from a non-moving harmonic load: (a) displacement and (b) phase.

of propagating waves can be realised away from the excitation point. Fig. 4, shows the track responses at 40 m away from the excitation point. It can be seen that the response below 19 Hz is small as it is dominated by evanescent waves and leaky waves which decay dramatically with distance. Fig. 4b shows that at the range of frequency between the two cut-on frequencies, both the rails and slab move in phase. Above the second cut-on frequency, the picture is complicated as two propagating waves contribute to the track displacement as can be seen from Fig. 2.

A different way of calculating the dispersion curves for a track under moving loads is by directly solving the equation $f_1(\xi, \omega = \varpi - \xi v) = 0$. At a given excitation frequency ϖ, this results in eight eigenvalues ξ_n ($n = 1,2,\ldots,8$). Due to the factor $e^{i\xi_n(x-vt)}e^{i\varpi t}$ in Eqs. (13)–(16), the value of ξ_n determines the wave type, whether propagating, leaky or evanescent, but in a moving frame of reference $x-vt$ (see the appendix for more details). At a given positive ϖ, a positive real root ξ_n represents a wave propagating to the right ahead of the moving load. In absence of damping, the velocity $v = 0$ gives the dispersion curves plotted before in Fig. 2. Dispersion curves for $v = 0$ are symmetrical about $\xi = 0$. This means that waves that propagate to the left are identical to those that propagate to the right. When considering damping in the calculations (provided by c_1 and c_2) for non-moving loads, all roots shift to new positions by rotating counter clockwise in the complex ξ domain. Hence, positive real roots of ξ_n gain small positive imaginary part and negative real roots of ξ_n gain small negative imaginary part. Thus propagating waves transform to leaky waves with small coefficients of attenuation.

Fig. 5 shows the dispersion curves for $v = 300\,\mathrm{m\,s^{-1}}$, where only positive frequencies are plotted. The dispersion curves are no longer symmetrical about $\xi = 0$. Compared with the non-moving load, the curves have moved down and to the left. Cut-on frequencies are lower than before and wavenumbers are longer ahead of the load than behind the load. This means that wavelengths are shorter in front of the load. At frequencies just above the first cut-on, waves with longer wavelengths have negative phase velocities. However, these waves still propagate away from the load as they have positive group velocities, see Ref. [29] for more details.

By increasing the load velocity more and more, the lower dispersion curve heads toward the wavenumber axis and touches it around $385\,\mathrm{m\,s^{-1}}$ (the same critical velocity as calculated before from Fig. 2). At this velocity, waves propagate from a constant moving load, i.e. a load with $\varpi = 0$.

The critical load velocity can also be calculated by plotting the displacement of the rails as a function of the load velocity as shown in Fig. 6. The critical load velocity from this figure occurs at about $380\,\mathrm{m\,s^{-1}}$, i.e. slightly smaller than the value calculated before and the difference is attributed to damping which is modelled in the calculations of Fig. 6. This figure also shows that the velocity effect is negligible when modelling

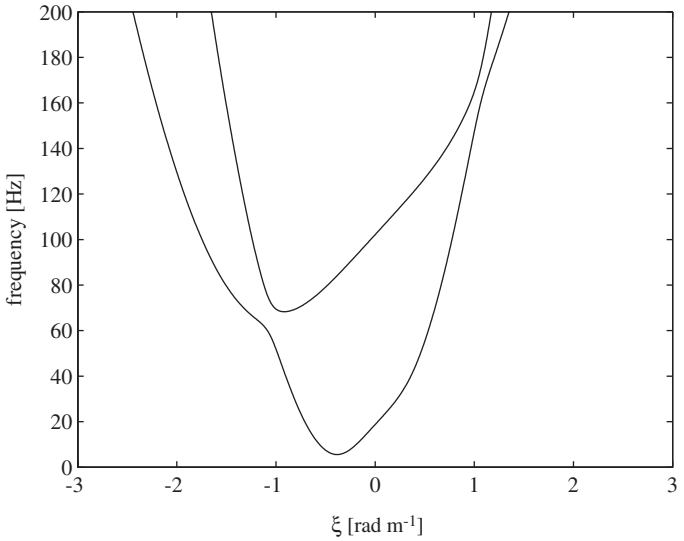

Fig. 5. Dispersion curves for floating-slab track under an oscillating moving load with $300\,\mathrm{m\,s^{-1}}$.

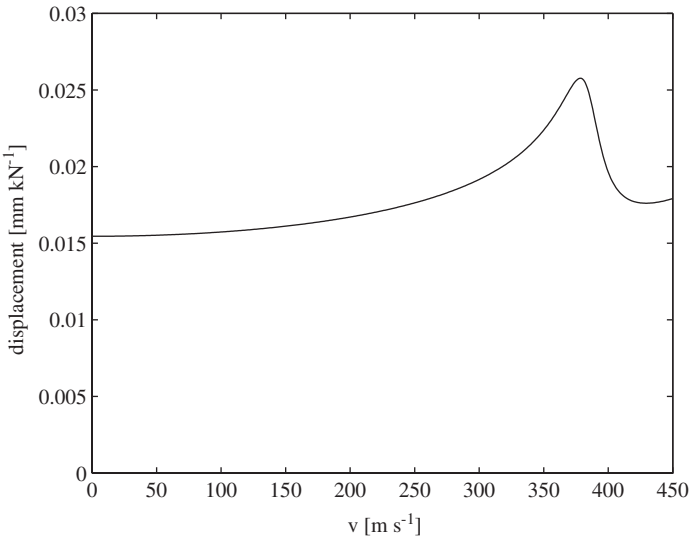

Fig. 6. Rail displacement under non-oscillating moving load. Critical velocity occurs at $380\,\mathrm{m\,s^{-1}}$.

non-oscillating moving loads on floating-slab tracks. This is true up to $100\,\mathrm{m\,s^{-1}}$, where no difference is observed between the static solution and the moving load solution. For underground trains, $100\,\mathrm{m\,s^{-1}}$ is much higher than typical train velocities.

In the previous discussion, wave propagation is considered in a moving frame of reference. For a propagating wave with angular frequency ϖ and wavenumber ξ_n, the observation point oscillates with angular frequency ϖ in a moving frame of reference. However, in a fixed frame of reference, it oscillates with angular frequency $\varpi-\xi_n v$. This can be shown from the following relationship

$$e^{i\varpi t}e^{i\xi_n(x-vt)} = e^{i(\varpi-\xi_n v)t}e^{i\xi_n x}. \tag{19}$$

Hence, for a fixed frame of reference, the oscillation frequency ω_n of the observation point can be written as

$$\omega_n = \varpi - \xi_n v = \varpi\big(1 - \xi_n v/\varpi\big) = \varpi\big(1 - v/c_n\big)$$

or

$$f_n = \bar{f}\left(1 - v/c_n\right), \tag{20}$$

where f_n is the oscillation frequency for a fixed frame of reference, $\bar{f}$ is the oscillation frequency for a moving frame of reference, and c_n is the phase velocity of the propagating wave. Eq. (20) is known physically as *Doppler effect*, see Ref. [30] for example. c_n can be positive or negative depending on the direction of propagation.

It is worth at this point commenting on the effect of coupling a discrete model of a train to a floating-slab track with a smooth rail-head. A simple model of a moving train is obtained by considering an axle moving over the track with constant velocity v. From Eq. (13–16), the displacements y_1, y_2 in a moving frame of axis ($z = x - vt$) under a moving load are invariant with time for $\varpi = 0$. This can be shown by substituting $x - vt = c$, where c is a constant. Therefore, for a non-oscillating moving load with a constant velocity, an observer who is moving along the rail with velocity equal to the load velocity keeps seeing the same deflected shapes of the rail and the slab. As a linear model, the steady-state deflection of the rail under a constant moving load increases proportionally to any increase in the magnitude of the load. Hence, for a moving axle on the track, the deflection of the rail at any point can be calculated by multiplying the deflection calculated for a unit load by the axle weight, i.e. $-Mg$, where M is the total axle mass and g is the gravity acceleration. Note that the axle inertia has an effect only on the transient displacement, i.e. when the axle starts to move. After some time, the transient effect disappears due to damping and only the steady-state effect remains. In reality, other loading mechanisms contribute to the axle–track interaction, which are not considered here. These are caused for instance by rail and wheel unevenness or roughness, rail joints, wheel flats and sleeper spacing.

4. Conclusions

Floating-slab tracks with continuous slabs are modelled in this paper. The track displacements under oscillating moving loads are calculated using the Fourier transformation method. Analysis of the dispersion curves is carried out to identify the track resonance frequencies. The critical load velocity is identified using a direct solution of the dispersion equation or by using the load-velocity line and the dispersion curves. For a track with no irregularities, such as roughness and rail joints, it is shown that no dynamic forces are induced at the wheel–track interface for a vehicle moving with a constant velocity. Moreover, no difference is observed between the static solution and the moving load solution for typical parameters of a track in underground tunnel.

Appendix A. Wavenumber-frequency domain analysis

The purpose of this appendix is to demonstrate some basic concepts about wave propagation and coupling of structures in the wavenumber-frequency domain. This is done by analysing the same model of the railway track used before but under a non-moving oscillating load. Three methods are presented in this appendix: the direct method, the Fourier transformation method and the coupling in the wavenumber-frequency domain method.

A.1. The direct method

This method treats the input force as a boundary condition for the problem. The model is shown in Fig. 7 with a concentrated harmonic load applied at $x = 0$. The model is split into two semi-infinite structures (left and right of $x = 0$). The input force is described for the right semi-infinite structure as a boundary condition on its left end. For the left semi-infinite structure the input force is described as a boundary condition on its right end. In this way, no forces are applied along the structures apart from at their ends. Due to symmetry, it is enough to analyse only the right semi-infinite structure.

For the element of length dx at distance x from the origin as shown in Fig. 7a, equations of motion read

$$EI_1 \frac{\partial^4 y_1}{\partial x^4} + m_1 \frac{\partial^2 y_1}{\partial t^2} = -k_1\left(y_1 - y_2\right) \tag{A.1}$$

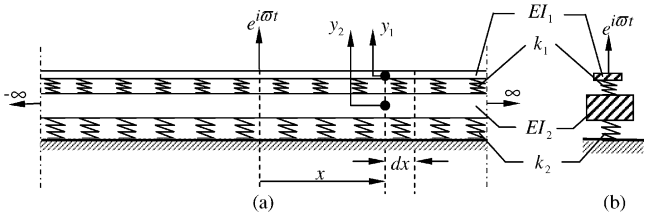

Fig. 7. A floating-slab track subjected to a harmonic load at $x = 0$: (a) front view and (b) side view at $x = 0$.

and

$$EI_2 \frac{\partial^4 y_2}{\partial x^4} + m_2 \frac{\partial^2 y_2}{\partial t^2} = k_1(y_1 - y_2) - k_2 y_2, \tag{A.2}$$

where EI_1 is the bending stiffness of both of the rails, EI_2 is the bending stiffness of the floating slab, k_1 is the stiffness of the railpads per unit length, k_2 is the stiffness of the slab bearings per unit length, m_1 is mass of the rails per unit length, m_2 is the mass of the floating slab per unit length, y_1 is the upper beam displacement, i.e. the rails displacement, and y_2 is the lower beam displacement, i.e. the slab displacement. Eqs. (A.1) and (A.2) can be written in matrix form as

$$\begin{bmatrix} EI_1 & 0 \\ 0 & EI_2 \end{bmatrix} \frac{\partial^4 y}{\partial x^4} + \begin{bmatrix} m_1 & 0 \\ 0 & m_2 \end{bmatrix} \frac{\partial^2 y}{\partial t^2} + \begin{bmatrix} k_1 & -k_1 \\ -k_1 & k_1 + k_2 \end{bmatrix} \mathbf{y} = \begin{bmatrix} 0 \\ 0 \end{bmatrix} \tag{A.3}$$

where $\mathbf{y} = [y_1, y_2]^{\mathrm{T}}$.

The following wave form solution is assumed for $\mathbf{y}$

$$\mathbf{y} = \begin{bmatrix} y_1 \\ y_2 \end{bmatrix} = \begin{bmatrix} Y_1 \\ Y_2 \end{bmatrix} \mathrm{e}^{\mathrm{i}(\omega t + \xi x)} = \mathbf{Y} \mathrm{e}^{\mathrm{i}(\omega t + \xi x)}. \tag{A.4}$$

Note that in the theory of differential equations, solution (A.4) is known as a homogeneous solution of the equations in Eq. (A.3). This also forms a general solution, as the particular solution is equal to zero (due to the zero vector on the right-hand side of Eq. (A.3)).

Substituting $\mathbf{y}$ from Eq. (A.4) in Eq. (A.3) results in

$$\begin{bmatrix} EI_1 \xi^4 + k_1 - m_1 \omega^2 & -k_1 \\ -k_1 & EI_2 \xi^4 + k_1 + k_2 - m_2 \omega^2 \end{bmatrix} \mathbf{Y} = \begin{bmatrix} 0 \\ 0 \end{bmatrix} \quad \text{or} \quad \mathbf{AY} = 0. \tag{A.5}$$

Eq. (A.5) has two possible solutions:

- a trivial solution, i.e. $\mathbf{Y} = 0$, where there are no displacements;
- a non-trivial solution, for this case $|\mathbf{A}| = 0$, i.e. the determinant of matrix $\mathbf{A}$ is equal to zero.

The determinant of matrix $\mathbf{A}$, is a function of ω, ξ and the track parameters: EI_1, EI_2, m_1, m_2, k_1 and k_2. The equation $|\mathbf{A}| = 0$ is known as the *Dispersion equation*. For prescribed track parameters, it is a function of ξ and ω. It will be seen later that the angular frequency ω must equal the excitation frequency ϖ, see Fig. 7. For a positive real value of ω, there are three different wave-type solutions according to the value of ξ in Eq. (A.4):

1. *propagating wave*: this solution arises when ξ is a real quantity. Positive real ξ results in a wave propagating to the left, while negative value results in a wave propagating to the right due to the factor $\mathrm{e}^{\mathrm{i}(\omega t + \xi x)}$ in Eq. (A.4);
2. *evanescent waves*: this solution arises when ξ is an imaginary quantity. Positive imaginary ξ results in a decaying solution with distance x, while negative imaginary ξ results in an increasing solution with x;

3. *leaky waves*: this solution arises when ξ is a complex quantity. The solution is propagating (oscillating) but with some decay/increase with distance. The sign of the real part of ξ determines the wave direction while the sign of the imaginary part of ξ determines whether the solution decays or increases with distance.

For the current problem and for a given angular frequency $\omega = \varpi$, the dispersion equation is a polynomial of the eighth order in ξ. The general displacements of the track can be written as

$$\mathbf{y} = \left(a_1\mathbf{E}_1 e^{i\xi_1 x} + a_2\mathbf{E}_2 e^{i\xi_2 x} + \cdots + a_8\mathbf{E}_8 e^{i\xi_8 x}\right)e^{i\omega t}. \tag{A.6}$$

The eigenvector $\mathbf{E}_n$ ($n = 1, 2, \ldots, 8$) is calculated from the following relationship

$$\mathbf{E}_n = \mathbf{D}(2), \tag{A.7}$$

where $\mathbf{D}(2)$ is the second column of the 2×2 matrix $\mathbf{D}$ which is calculated by

$$[\mathbf{S}, \mathbf{V}, \mathbf{D}] = svd(\mathbf{A}_n), \tag{A.8}$$

where the right-hand side is the singular value decomposition of matrix $\mathbf{A}$ evaluated at the solution (ξ_n, ω), see Ref. [31] for more details.

In Fig. 8a, solutions of the dispersion equation are plotted at each frequency $f = \omega/(2\pi)$ for the range of frequency 0–100 Hz, using the track parameters given in Table 1.

At low frequencies, it can be seen from Fig. 8a and b that there are no real solutions ξ and hence the track displacements do not include propagating waves. For higher frequencies (see Fig. 8a and c) real solutions of ξ appear. The frequency at which waves start to propagate is known as the *cut-on frequency*. This frequency is 18.75 Hz for the current parameters.

The final step in this method is to find the coefficients $a_1, a_2, \ldots, a_8$ in Eq. (A.6) by using the boundary conditions.

For the right semi-infinite structure, i.e. for $x > 0$, any coefficient a_n associated with solutions increasing with x should be set to zero, as the displacement does not increase with distance away from the excitation point. Moreover, purely propagating waves should travel only to the right due to absence of sources at $x > 0$, and hence any coefficient associated with real positive ξ should be set to zero. This means for $x > 0$, only solutions associated with ξ which lie in the first and the second quarter excluding the positive real axis are included in the displacement, which is applicable on four roots (see Fig. 8). A similar argument can be used for the left semi-infinite beams, where this time only roots which lie in the third and the forth quarter excluding the negative real axis are included in the displacement.

The remaining four coefficients in Eq. (A.6) are determined by using the boundary conditions at $x = 0$. There are four boundary conditions at $x = 0$ due to symmetry and are expressed mathematically in Eq. (A.9): the slope is zero for the upper and the lower beams and the shear force is equal to half of the applied force for the upper and the lower beam, i.e. $F/2$ and zero respectively. Note that the shear force condition at $x = 0$ for the upper beam is only satisfied if $\omega = \varpi$.

$$\frac{\partial y_1(x=0,t)}{\partial x} = 0, \tag{A.9a}$$

$$\frac{\partial y_2(x=0,t)}{\partial x} = 0, \tag{A.9b}$$

$$EI_1 \frac{\partial^3 y_1(x=0,t)}{\partial x^3} = \frac{F}{2}, \tag{A.9c}$$

and

$$EI_2 \frac{\partial^3 y_2(x=0,t)}{\partial x^3} = 0. \tag{A.9d}$$

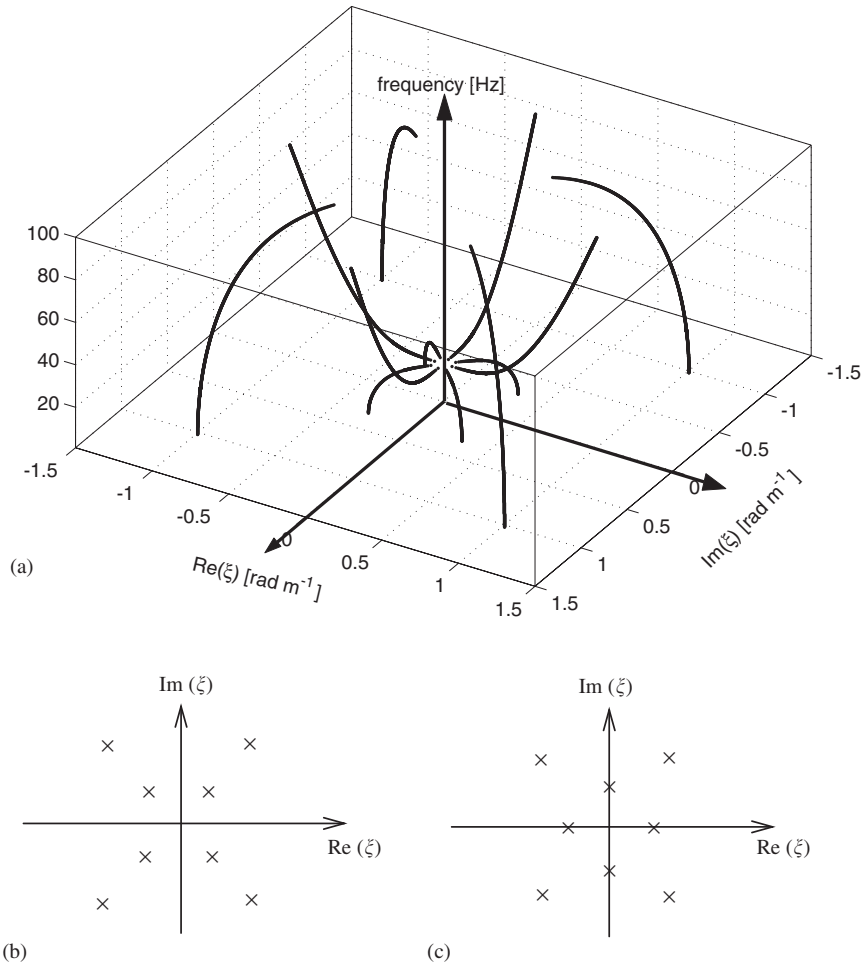

Fig. 8. (a) Roots of the dispersion equation of a floating-slab track on rigid foundation, where the real part and imaginary part of a complex wavenumber ξ are abbreviated by Re(ξ) and Im(ξ) respectively. (b) Cross-sectional view of (a) at frequency below the cut-on frequency, where all solutions are complex quantities. (c) Cross-sectional view of (a) at frequency above the cut-on frequency, where four solutions are complex, two are real and two are imaginary quantities. The ($\times$) sign shows a root position.

A.2. The Fourier transformation method

Unlike the direct method, this method treats the load as a part of the differential equation rather than a boundary condition. In this method, the governing differential equations of the track are transformed to the wavenumber-frequency domain (ξ,ω). The transformed equations are then simplified and transformed back to the space–time domain (x,t). For the model shown in Fig. 7, the governing differential equations (equivalent to Eqs. (A.1 and A.2)) read

$$EI_1 \frac{\partial^4 y_1}{\partial x^4} + m_1 \frac{\partial^2 y_1}{\partial t^2} + k_1 (y_1 - y_2) = \delta(x) e^{i\omega t} \tag{A.10}$$

and

$$EI_2 \frac{\partial^4 y_2}{\partial x^4} + m_2 \frac{\partial^2 y_2}{\partial t^2} - k_1 (y_1 - y_2) + k_2 y_2 = 0. \tag{A.11}$$

Eqs. (A.10) and (A.11) are transformed to the wavenumber-frequency domain. The transformed equations read

$$EI_1\xi^4\tilde{y}_1 - m_1\omega^2\tilde{y}_1 + k_1\left(\tilde{y}_1 - \tilde{y}_2\right) = 2\pi\delta(\omega - \varpi) \tag{A.12}$$

and

$$EI_2\xi^4\tilde{y}_2 - m_2\omega^2\tilde{y}_2 - k_1\left(\tilde{y}_1 - \tilde{y}_2\right) + k_2\tilde{y}_2 = 0. \tag{A.13}$$

Eqs. (A.12) and (A.13) can be written in matrix form as

$$\begin{bmatrix} EI_1\xi^4 + k_1 - m_1\omega^2 & -k_1 \\ -k_1 & EI_2\xi^4 + k_1 + k_2 - m_2\omega^2 \end{bmatrix}\tilde{\mathbf{y}} = \begin{bmatrix} 2\pi\delta(\omega - \varpi) \\ 0 \end{bmatrix}, \tag{A.14}$$

where $\tilde{\mathbf{y}} = \left[\tilde{y}_1, \tilde{y}_2\right]^{\mathrm{T}}$. Note that the matrix on the left-hand side is matrix $\mathbf{A}$ in Eq. (A.5). The inverse of matrix $\mathbf{A}$ can be written as

$$\mathbf{A}^{-1} = \frac{1}{|\mathbf{A}|}\begin{bmatrix} EI_2\xi^4 + k_1 + k_2 - m_2\omega^2 & k_1 \\ k_1 & EI_1\xi^4 + k_1 - m_1\omega^2 \end{bmatrix}. \tag{A.15}$$

Eq. (A.14) can be written as

$$\tilde{\mathbf{y}}(\xi, \omega) = \frac{2\pi\delta(\omega - \varpi)}{|\mathbf{A}|}\begin{bmatrix} EI_2\xi^4 + k_1 + k_2 - m_2\omega^2 \\ k_1 \end{bmatrix}. \tag{A.16}$$

Transforming Eq. (A.16) firstly to the wavenumber-time domain results in

$$\bar{\mathbf{y}}(\xi, t) = \frac{\mathrm{e}^{\mathrm{i}\varpi t}}{|\mathbf{A}|_{@\omega=\varpi}}\begin{bmatrix} EI_2\xi^4 + k_1 + k_2 - m_2\varpi^2 \\ k_1 \end{bmatrix}. \tag{A.17}$$

Now, Eq. (A.17) is transformed to the space–time domain

$$\mathbf{y}(x, t) = \frac{\mathrm{e}^{\mathrm{i}\varpi t}}{2\pi}\int_{-\infty}^{\infty}\frac{1}{|\mathbf{A}|_{@\omega=\varpi}}\begin{bmatrix} EI_2\xi^4 + k_1 + k_2 - m_2\varpi^2 \\ k_1 \end{bmatrix}\mathrm{e}^{\mathrm{i}\xi x}\,\mathrm{d}\xi. \tag{A.18}$$

It is sufficient for the purpose of demonstration to solve for $y_1(x,t)$ as $y_2(x,t)$ can be found using the same procedure. From Eq. (A.18), $y_1(x,t)$ can be written as

$$y_1(x, t) = \frac{\mathrm{e}^{\mathrm{i}\varpi t}}{2\pi}\int_{-\infty}^{\infty} f(\xi)\mathrm{e}^{\mathrm{i}\xi x}\,\mathrm{d}\xi, \tag{A.19}$$

where $f(\xi) = \left[\left(EI_2\xi^4 + k_1 + k_2 - m_2\varpi^2\right)/\left(|A|_{@\omega=\varpi}\right)\right]$. There are two methods for evaluating the integration in Eq. (A.19). The first is by performing the integration directly on the real ξ-axis. This is difficult to undertake analytically and hence it may be calculated numerically using the IDFT, i.e. the inverse discrete Fourier transform. The other method is to use the results of contour integration from the theory of complex variables, see Ref. [32] for example. As shown in Fig. 9, the integration of the function $f(\xi)\mathrm{e}^{\mathrm{i}\xi x}$ along the real axis from $\xi_a \to -\infty$ to $\xi_b \to \infty$, is equivalent to the closed-path integration along the real axis from ξ_a to ξ_b plus the integration along the semicircle from ξ_b to ξ_a, provided that the integration along the semicircle is zero. This integration along this closed path is equal to the summation of residues evaluated at the poles of the function $f(\xi)\mathrm{e}^{\mathrm{i}\xi x}$, i.e.

$$\int_{-\infty}^{\infty} f(\xi)\mathrm{e}^{\mathrm{i}\xi x}\,\mathrm{d}\xi = 2\pi i\sum_{n=1}^{n=N}\mathrm{Res}\left[f(\xi)\mathrm{e}^{\mathrm{i}\xi x}, \xi_n\right], \tag{A.20}$$

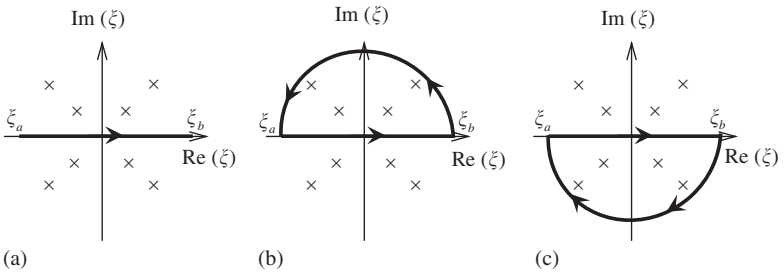

Fig. 9. The integration of the function $f(\xi)e^{i\xi x}$ along the real axis from $\xi_a \to -\infty$ to $\xi_b \to -\infty$ in (a) is equivalent to the integration along the real axis from ξ_a to ξ_b plus the semicircle from ξ_b to ξ_a in (b) or (c). The choice depends upon whether the integration along the semicircle is zero.

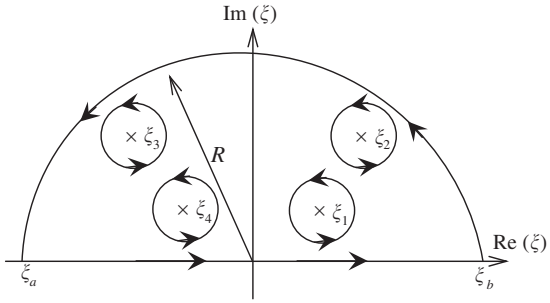

Fig. 10. The integration of the function $f(\xi)e^{i\xi x}$ on the closed contour along the real axis from ξ_a to ξ_b plus the semicircle from ξ_b to ξ_a is equivalent to the sum of integrations along the closed paths around the poles which lie inside the closed contour. The integration around a pole ξ_n is calculated by $2\pi i\,\mathrm{Res}[f(\xi)e^{i\xi x}, \xi_n]$.

where $\mathrm{Res}[f(\xi)e^{i\xi x},\xi_n]$ is the residue of $f(\xi)e^{i\xi x}$ at the pole ξ_n, N is the total number of poles enclosed by the contour. The poles of $f(\xi)e^{i\xi x}$ are the singular points of the function and can be calculated by equating the denominator of $f(\xi)$ to zero, i.e.

$$|A|_{@\omega=\varpi} = 0. \tag{A.21}$$

The last equation is identical to the dispersion equation as calculated in the previous section (note in the previous section that $\omega = \varpi$). As mentioned before, this equation has eight solutions at any angular frequency $\omega = \varpi$ and they are plotted in Fig. 8.

The integration along the semicircle in Fig. 9 (substituting $\xi = Re^{i\theta}$) is

$$\int f(\xi)e^{i\xi x}\,\mathrm{d}\xi = \int_{\theta=0}^{\theta=\pi} \frac{EI_2\left(Re^{i\theta}\right)^4 + k_1 + k_2 - m_2\omega^2}{|A|_{@\omega=\varpi}} (Rie^{i\theta})\left(e^{i(R\cos\theta + iR\sin\theta)x}\right)\mathrm{d}\theta. \tag{A.22}$$

The factor $e^{-Rx\sin\theta}$ in the last integration determines whether the integration will approach infinity or zero when R tends to infinity. In the first and the second quarter $\sin\theta > 0$ and the integration only tends to zero for positive values of x. Thus for $x > 0$, the closed integration in Fig. 9b is used. For $x < 0$ a different contour is used, in which the semicircle passes through the third and fourth quarter, see Fig. 9c. In this way, the integration along the semicircle part always tends to zero when R tends to infinity.

Once the path is chosen, the integration along a closed contour is replaced by a summation of the residues at the interior poles [32]. For the current problem if none of the poles lies on the real axis (Fig. 10), Eq. (A.19) can be simplified to

$$y_1(x,t) = 2\pi i \frac{e^{i\varpi t}}{2\pi} \sum_{n=1}^{n=4} \left(\frac{EI_2\xi_n^4 + k_1 + k_2 - m_2\varpi^2}{EI_1EI_2\prod_n} \right) e^{i\xi_n x} \quad \text{for } x \geqslant 0, \tag{A.23a}$$

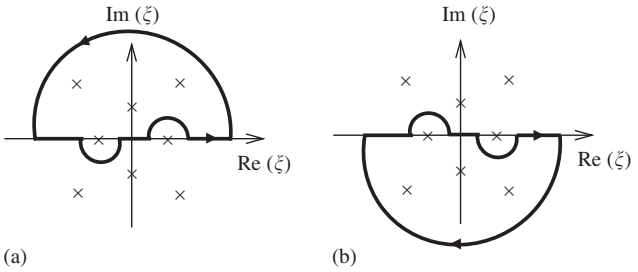

Fig. 11. The contour path for a frequency above the cut-on frequency, where some poles (solutions) lie on the real axis: (a) for $x \geqslant 0$ and (b) for $x < 0$.

and

$$y_1(x,t) = -2\pi i \frac{e^{i\varpi t}}{2\pi} \sum_{n=5}^{n=8} \left(\frac{EI_2\xi_n^4 + k_1 + k_2 - m_2\varpi^2}{EI_1EI_2\prod_j} \right) e^{i\xi_n x} \quad \text{for } x<0, \tag{A.23b}$$

where

$$\prod_n = (\xi_n - \xi_1)(\xi_n - \xi_2)\ldots(\xi_n - \xi_{n-1})(\xi_n - \xi_{n+1})\ldots(\xi_n - \xi_8),$$

$\xi_1, \xi_2, \ldots, \xi_8$ are the roots of dispersion equation at $\omega = \varpi$, ξ_1, ξ_2, ξ_3, ξ_4 are the roots in the first and the second quadrants, and ξ_5, ξ_6, ξ_7, ξ_8 are the roots in the third and the fourth quadrants.

The additional minus sign in Eq. (A.23b) is to account for the clockwise direction of the contour around the poles, see Fig. 9c.

For frequencies above the cut-on frequency some poles lie on the real axis and the integration path is modified to include or exclude the pole using the same physical argument used in the previous section. Fig. 11 shows the appropriate contour for $x \geqslant 0$ and $x < 0$ for the case in Fig. 8c, i.e. for a frequency above the cut-on frequency. For instance, in Fig. 11a the positive real value root is excluded by a small semicircle as it produces a propagating wave to the left due to the factor ($e^{i\varpi t}e^{i\xi x}$) in Eq. (A.23a).

Note that the displacement in Eqs. (A.23a) and (A.23b) comprises of the three wave-type solutions discussed before, i.e. propagating, evanescent and leaky waves. It can be proved that this solution is identical to the one calculated by the direct method in the previous section.

A.3. Coupling in the wavenumber-frequency domain

The method of coupling in the wavenumber-frequency domain is demonstrated in this section by analysing the floating-slab track in Fig. 7. The model is split into two structures. The first structure is the upper beam as shown in Fig. 12b, which accounts for the rails. The second structure is a beam on elastic foundation as shown in Fig. 12c, which accounts for the floating slab and the slab bearings. These two structures are coupled via railpads which are uniformly distributed longitudinally throughout the length.

An essential part of the analysis is to find the *frequency response functions* (FRFs) of the two structures separately in the wavenumber-frequency domain.

The generalised differential equation for the first structure, i.e. a free Euler–Bernoulli beam is

$$EI_1 \frac{\partial^4 z_1}{\partial x^4} + m_1 \frac{\partial^2 z_1}{\partial t^2} = P_1, \tag{A.24}$$

where z_1 is the vertical displacement of the free beam and P_1 is the total force on the beam in the vertical direction.

There are two methods for calculating the FRF of this structure:

1. Transforming the differential equation to the wavenumber-frequency domain directly using double Fourier transform [28], which results in

$$EI_1\xi^4\tilde{z}_1 - m_1\omega^2\tilde{z}_1 = \tilde{P}_1. \tag{A.25}$$

The displacement FRF of the free beam is defined as the vertical displacement of the free beam for a unit vertical load in the wavenumber-frequency domain. Applying this definition on Eq. (A.25), results in

$$\tilde{H}_{11} = \frac{\tilde{z}_1}{\tilde{P}_1} = \frac{1}{EI_1\xi^4 - m_1\omega^2}. \tag{A.26}$$

2. By using the following expressions for the displacement and force

$$z_1 = \tilde{z}_1 e^{i(\xi x+\omega t)} \quad \text{and} \quad P_1 = \tilde{P}_1 e^{i(\xi x+\omega t)}. \tag{A.27}$$

Substituting these expressions of z_1 and P_1 in Eq. (A.24), results in the displacement FRF of the free beam as in Eq. (A.26).

To explain why the two methods lead to the FRF, consider the force in Eq. (A.25), i.e. $\tilde{P}_1$. This force is in the wavenumber-frequency domain and concentrated at specific wavenumber ξ and angular frequency ω. It can be expressed as a function in the wavenumber-frequency domain (ξ_0,ω_0) as $\tilde{P}_1\delta(\xi_0 - \xi)\delta(\omega_0 - \omega)$, where (ξ_0, ω_0) are used in this context to express the wavenumber-frequency coordinates. Transforming this expression to the space–time domain

$$\frac{1}{(2\pi)^2}\int_{\omega_0=-\infty}^{\infty}\int_{\xi_0=-\infty}^{\infty} \tilde{P}_1\delta(\xi_0 - \xi)\delta(\omega_0 - \omega)e^{i(\xi_0 x+\omega_0 t)}\,d\xi_0\,d\omega_0 = \frac{1}{(2\pi)^2}\tilde{P}_1 e^{i(\xi x+\omega t)}. \tag{A.28}$$

In the same way the transformation of the displacement in Eq. (A.25) to the space–time domain gives

$$\frac{1}{(2\pi)^2}\int_{\omega_0=-\infty}^{\infty}\int_{\xi_0=-\infty}^{\infty} \tilde{z}_1\delta(\xi_0 - \xi)\delta(\omega_0 - \omega)e^{i(\xi_0 x+\omega_0 t)}\,d\xi_0\,d\omega_0 = \frac{1}{(2\pi)^2}\tilde{z}_1 e^{i(\xi x+\omega t)}. \tag{A.29}$$

By multiplying the input and the output in Eqs. (A.28) and (A.29) by $(2\pi)^2$, it can be seen that the FRF calculated by the second method is equivalent to the one calculated by the first method.

For the second structure, i.e. a beam on elastic foundation, the generalised differential equation in the space–time domain reads

$$EI_2\frac{\partial^4 z_2}{\partial x^4} + m_2\frac{\partial^2 z_2}{\partial t^2} + k_2 z_2 = P_2, \tag{A.30}$$

where z_2 is the vertical displacement of the beam and P_2 is the applied force on the beam in the vertical direction.

To calculate the FRF of this structure, substitute $z_2 = \tilde{z}_2 e^{i(\xi x+\omega t)}$ and $P_2 = \tilde{P}_2 e^{i(\xi x+\omega t)}$ and rearrange to get

$$\tilde{H}_{22} = \frac{\tilde{z}_2}{\tilde{P}_2} = \frac{1}{EI_2\xi^4 - m_2\omega^2 + k_2}, \tag{A.31}$$

where $\tilde{H}_{22}$ is the FRF of the beam on elastic foundation in Fig. 12c.

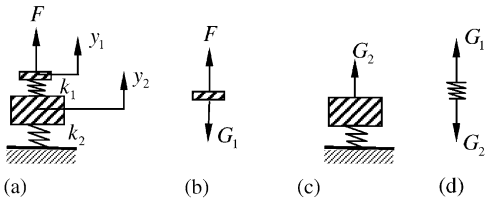

Fig. 12. Coupling of structures in the wavenumber-frequency domain: (a) the coupled structure; (b) the first structure: a free beam; (c) the second structure: a beam on an elastic foundation; and (d) the railpads which connect the two structures.

It is possible now to couple the two structures. For the vertical equilibrium of forces in the space–time domain, one can write (see Fig. 12d)

$$G_1 = G_2 = G. \tag{A.32}$$

This equation is transformed to the wavenumber-frequency domain by substituting $G_1 = \tilde{G}_1 e^{i(\xi x+\omega t)}$, $G_2 = \tilde{G}_2 e^{i(\xi x+\omega t)}$ and $G = \tilde{G} e^{i(\xi x+\omega t)}$ to give

$$\tilde{G}_1 = \tilde{G}_2 = \tilde{G}. \tag{A.33}$$

The rest of the analysis is carried out directly in the wavenumber-frequency. The equations of motion are written for the two structures and the railpads as follows

$$\tilde{y}_1 = \tilde{H}_{11}\big(\tilde{F} - \tilde{G}\big), \tag{A.34}$$

$$\tilde{y}_2 = \tilde{H}_{22}\tilde{G}, \tag{A.35}$$

and

$$\tilde{G} = k_1\big(\tilde{y}_1 - \tilde{y}_2\big). \tag{A.36}$$

Solving Eqs. (A.34), (A.35) and (A.36) for $\tilde{y}_1$ results in

$$\tilde{y}_1 = \frac{\tilde{H}_{11}\big(1 + k_1\tilde{H}_{22}\big)\tilde{F}}{1 + k_1\big(\tilde{H}_{11} + \tilde{H}_{22}\big)}. \tag{A.37}$$

Substituting $\tilde{H}_{11}$ and $\tilde{H}_{22}$ from Eqs. (A.26) and (A.31) and for a unit harmonic load applied at $x = 0$ with angular frequency ϖ, i.e. $\tilde{F} = 2\pi\delta(\omega - \varpi)$, the equation reduces to the value of $\tilde{y}_1$ as calculated by Eq. (A.16).

References

[1] P. Grootenhuis, Floating track slab isolation for railways, *Journal of Sound and Vibration* 51 (3) (1977) 443–448.
[2] G.P. Wilson, H.J. Saurenman, J.T. Nelson, Control of ground-borne noise and vibration, *Journal of Sound and Vibration* 87 (2) (1983) 339–350.
[3] J.T. Nelson, Recent developments in ground-borne noise and vibration control, *Journal of Sound and Vibration* 193 (1) (1996) 367–376.
[4] J.A. Forrest, Modelling of Ground Vibration from Underground Railways, PhD Dissertation, Cambridge University, 1999.
[5] L. Fryba, History of Winkler foundation, *Vehicle System Dynamics Supplement* 24 (1995) 7–12.
[6] A.E.H. Love, *A Treatise on the Mathematical Theory of Elasticity*, Dover, New York, 1944.
[7] S. Timoshenko, Methods of analysis of statical and dynamical stresses in rail, *Proceedings of the Second International Congress of Applied Mechanics*, Zurich, 1926, pp. 407–418.
[8] B.K. Hovey, *Beitrag zur Dynamik des geraden Eisenbahngleises, Dissertation*, Göttingen Universitaet, Germany, 1933.
[9] K. Ludwig, Deformation of a rail elastically supported and of infinite length by loads moving at a constant horizontal velocity, *Proceedings of the Fifth International Congress of Mechanics*, 1938, p. 650.
[10] J. Dorr, Der unendlich, federnd gebettete Balken unter dem Einflu\einer gleichformig bewegten Last, *Ingenieur-Archiv* 14 (3) (1943) 167–192.
[11] J.T. Kenny, Steady-state vibrations of beams on elastic foundation for moving load, *Journal of Applied Mechanics* 21 (1954) 359–364.
[12] P.M. Mathews, Vibrations of a beam on elastic foundation, *Zeitschrift für Angewandte Mathematik und Mechanik* 38 (1958) 105–115.
[13] P.M. Mathews, Vibrations of a beam on elastic foundation II, *Zeitschrift für Angewandte Mathematik und Mechanik* 39 (1959) 13–19.
[14] S. Chonan, Moving harmonic load on an elastically supported Timoshenko beam, *Zeitschrift für Angewandte Mathematik und Mechanik* 58 (1978) 9–15.
[15] R. Bogacz, T. Krzyzynski, K. Popp, On the generalization of Mathew's problem of the vibrations of a beam on elastic foundation, *ZAMM-Zeitschrift für Angewandte Mathematik und Mechanik* 69 (8) (1989) 243–252.
[16] S. Kim, J.M. Roesset, Dynamic response of a beam on a frequency-independent damped elastic foundation to moving load, *Canadian Journal of Civil Engineering* 30 (2003) 460–467.
[17] L. Fryba, *Vibration of Solids and Structures under Moving Loads*, Noordhoff Publishing, Groningen, 1972.
[18] D.G. Duffy, The response of an infinite railroad track to a moving, vibrating mass, *Journal of Applied Mechanics, Transaction of the American Society of Mechanical Engineers ASME* 57 (1990) 66–73.
[19] P.L. Pasternak, *Fundamentals of a new method of analysis of structures on elastic foundation by means of two subgrade coefficients*, Gosudarstvennoe Izdatel'stvo Literatury po Stroitel'stvu I Arkhitekture, Moscow, 1954 (in Russian).
[20] A.K. Mallik, S. Chandra, A.B. Singh, Steady state response of an elastically supported infinite beam to a moving load, *Journal of Sound and Vibrations* 291 (3–5) (2006) 1148–1169.

[21] P.G. Kessel, Resonances excited in an elastically connected double-beam system by a cyclic moving load, *Journal of Acoustical Society of America* 40 (1966) 684–687.
[22] H.V. Vu, A.M. Ordonez, B.H. Karnopp, *Vibration of a double-beam system. Journal of Sound and Vibration* 229 (4) (2000) 807–822.
[23] Seon M. Han, H. Benaroya, T. Wei, Dynamics of transversely vibrating beams using four engineering theories, *Journal of Sound and Vibration* 225 (5) (1999) 935–988.
[24] Y.-H. Chen, Z.-M. Shiu, Resonant curves of an elevated railway to harmonic moving loads, *International Journal of Structural Stability and Dynamics* 4 (2) (2004) 237–257.
[25] F. Cui, C.H. Chew, The effectiveness of floating slab track system—Part I, receptance method, *Applied Acoustics* 61 (2000) 441–453.
[26] H.E.M. Hunt, J.A. Forrest, Floating slab track for vibration reduction: why simple models don't work, *Proceedings of the Seventh International Congress on Sound and Vibration*, Garmisch-Partenkirchen, Germany, July 2000, CDROM.
[27] J.S. Chisholm, R.M. Morris, *Mathematical Methods in Physics*, North-Holland, Amsterdam, 1964.
[28] S. Stearns, *Digital Signal Analysis*, Hayden Book Company, Inc., New Jersey, 1983.
[29] K.F. Graff, *Wave motion in Elastic Solids*, Oxford University Press, London, 1975.
[30] A.B. Wood, *A Textbook of Sound*, G. Bell and Son Ltd., 1946.
[31] G. Strang, *Linear Algebra and its Application*, third ed., Harcourt Brace Jovanovich College Publishers, 1988.
[32] A.D. Wunsch, *Complex Variables with Applications,* Addison-Wesley, Reading, MA, 1983.